Journal of
Synchrotron
Radiation

ISSN 0909-0495

Received 29 October 2012
Accepted 24 December 2012

X-ray speckle visibility spectroscopy in the single-photon limit

Curt DeCaro,[a] Vidanage Nuwan Karunaratne,[a] Sambhunath Bera,[a] Laurence B. Lurio,[a]* Alec R. Sandy,[b] Suresh Narayanan,[b] Mark Sutton,[c] John Winans,[d] Kirk Duffin,[d] Jon Lehuta[d] and Nicholas Karonis[d,e]

[a]Department of Physics, Northern Illinois University, DeKalb, IL 60615, USA, [b]X-ray Science Division, Argonne National Laboratory, Argonne, IL 60439, USA, [c]Department of Physics, McGill University, Montréal, Québec, Canada H3A 2T8, [d]Department of Computer Science, Northern Illinois University, Dekalb, IL 60615, USA, and [e]Mathematics and Computer Science Division, Argonne National Laboratory, Argonne, IL 60439, USA. E-mail: llurio@niu.edu

The technique of speckle visibility spectroscopy has been employed for the measurement of dynamics using coherent X-ray scattering. It is shown that the X-ray contrast within a single exposure can be related to the relaxation time of the intermediate scattering function, and this methodology is applied to the diffusion of 72 nm-radius latex spheres in glycerol. Data were collected with exposure times as short as 2 ms by employing a resonant shutter. The weak scattering present for short exposures necessitated an analysis formalism based on the spatial correlation function of individual photon charge droplets on an area detector, rather than the usual methods employed for intensity correlations. It is demonstrated that this method gives good agreement between theory and experiment and thus holds promise for extending area-detector-based coherent scattering methods to the study of faster dynamics than previously obtainable.

Keywords: speckle visibility; dynamics; XPCS; droplet analysis.

1. Introduction

Coherent X-ray scattering provides a method to measure the equilibrium dynamics of materials in the realm of slow dynamics and short length scales. When a sample is illuminated with a coherent X-ray beam, the resulting scattering pattern is modulated by a random speckle pattern. The speckle intensities vary in time as the sample undergoes thermal fluctuations. In the most commonly applied technique of X-ray photon correlation spectroscopy (XPCS), an extension of laser-based photon correlation spectroscopy (PCS) (Pecora, 1985), the time correlation of the frame-to-frame intensity yields the dynamic structure factor of the sample being measured (Grubel *et al.*, 2008). For simple Brownian diffusion, the dynamic structure factor is an exponential decay with a time constant proportional to the diffusion constant. In more complicated cases, the dynamic structure factor gives detailed information about the microscopic sample dynamics (Pusey, 1991; Pecora, 1985). XPCS measurements require an intense coherent incident X-ray beam, and hence only became possible with the advent of third-generation synchrotron facilities. However, even in the case of undulator X-ray radiation from third-generation sources, XPCS measurements are often intensity limited.

A crucial innovation in the technique of XPCS which allowed flux limitations to be partially overcome is to use an area detector to collect scattering over a wide range of angles, but with a resolution sufficient to resolve intensity variations within individual speckles (Falus *et al.*, 2004; Westermeier *et al.*, 2009). The use of a megapixel area detector, where each pixel can subtend the same solid angle as a single-element point detector, yields an increase in signal-to-noise ratio (SNR) by the square root of the number of pixels, giving a thousandfold increase in SNR. Furthermore, even were there enough flux available to obtain adequate signal to noise with a point detector, an area detector has the significant advantage that owing to the larger solid angle the same SNR can be obtained with less sample damage. A limitation of area detectors is that they require significant time to read out, typically several milliseconds. This has prevented XPCS measurements from accessing sample dynamics in the submillisecond regime. This time domain is particularly relevant for the study of biomaterials which have so far not been addressed by XPCS methods.

A variation of XPCS which provides a means to access faster times than traditional XPCS is X-ray speckle visibility spectroscopy (XSVS). In this technique, rather than correlating the frame-to-frame intensity variations of a pixel, the visibility of speckles within each frame is characterized and the exposure time of a frame is varied to access information about time dependence. Since the main limitation of a CCD camera is readout time, this permits arbitrarily fast dynamics

to be measured as long as the camera can be rapidly shuttered.

For sufficiently short exposure times the scattering within a single frame usually consists of a small number of isolated photons, each of which leaves a small droplet of charge (usually a few pixels in size) on the camera. Under such weak illumination conditions it is advantageous to use a droplet algorithm to replace the charge droplets on the camera with a list of photon positions. Such a procedure has been employed previously by several authors (Chushkin *et al.*, 2012; Livet *et al.*, 2000; Hruszkewycz *et al.*, 2012). This has several advantages, including data compression, noise suppression and increased spatial resolution.

In the present work we have performed XSVS experiments on a prototypical colloidal system of polystyrene latex spheres diffusing in glycerol suspension. We employed a custom CCD camera as a detector (Denes *et al.*, 2009) with 237000 pixels. The pixels are 30 µm × 30 µm and the entire frame is read out in 10 ms. The camera has a depletion depth of 300 µm providing near 100% efficiency at the X-ray energy employed (7.35 keV). We also used a vibrating resonant shutter to achieve very short exposure times, as low as 2 ms. We demonstrate below that this provides sensitivity to dynamics approximately 20 times faster than could be accessed using XPCS methods.

2. Theory

In a standard XPCS experiment a sample is illuminated with a coherent or partially coherent X-ray beam which leads to a scattering pattern with a superimposed speckle pattern. The time autocorrelation function of the intensity within each speckle sized region is calculated and then this function is averaged over equivalent regions. The time autocorrelation is specifically defined by

$$g_2(\tau) \equiv \frac{\langle I(Q,t)I(Q,t+\tau)\rangle}{\langle I(Q)\rangle^2}. \quad (1)$$

Here, $Q = 4\pi\sin(\theta)/\lambda$ with 2θ the angle between the incident beam and scattered beam and λ is the X-ray wavelength. In the case of measurements made using a CCD camera with a large number of pixels and under the assumption that the sample is isotropic, the averaging implied by $\langle\ldots\rangle$ is usually performed by taking an average over both the time t and the equivilent pixels within a ring of scattering of magnitude Q and width ΔQ. Under the assumption that the length and time scales associated with the sample dynamics are well separated from the size of the beam and the time scale of intensity fluctuations within the beam, equation (1) can be related to the normalized intermediate scattering function $f(Q,\tau)$ (Grubel *et al.*, 2008),

$$g_2(\tau) = 1 + \beta f(Q,\tau)^2. \quad (2)$$

Here, β is the optical contrast of the experimental set-up, and the intermediate scattering function is given by $f(Q,\tau) = F(Q,\tau)/F(Q,0)$ with

$$F(\mathbf{Q},\tau) = \int \mathrm{d}^3\mathbf{r} \int \mathrm{d}^3\mathbf{r}'\, \rho(\mathbf{r},t)\rho(\mathbf{r}',t+\tau)\exp[i\mathbf{Q}\cdot(\mathbf{r}-\mathbf{r}')]. \quad (3)$$

Here, ρ is the scattering length density. For the case of simple diffusive motion one has $f(Q,\tau) = \exp(-DQ^2|\tau|)$ where D is the diffusion coefficient.

Even in a traditional XPCS experiment there is a correction to the correlation function due to the exposure time. Consider a sequence of N images taken with a finite exposure time t_e. Each product of intensities in the correlation function now represents an integral over a range of time differences within the two exposures. Specifically, the exact correlation function $g_2(\tau)$ is now approximated by a time-averaged correlation function $g_2'(\tau, t_\mathrm{e})$ given by

$$g_2'(\tau,t_\mathrm{e}) = \frac{1}{\langle I\rangle^2}\frac{1}{t_\mathrm{e}^2}\left\langle \int_t^{t+t_\mathrm{e}} \mathrm{d}t' \int_{t+\tau}^{t+\tau+t_\mathrm{e}} \mathrm{d}t''\, I(t')I(t'')\right\rangle. \quad (4)$$

This expression can be written in terms of the intermediate scattering function,

$$g_2'(\tau,t_\mathrm{e}) = 1 + \frac{\beta}{t_\mathrm{e}^2}\int_0^{t_\mathrm{e}} \mathrm{d}t' \int_\tau^{\tau+t_\mathrm{e}} \mathrm{d}t''\, f^2(t''-t'). \quad (5)$$

In the specific case where $f(\tau) = \exp(-\Gamma|\tau|)$, equation (5) can be analytically integrated to yield

$$g_2'(\tau,t_\mathrm{e}) = 1 + \beta\exp(-2\Gamma\tau)\left[\sinh(\Gamma t_\mathrm{e})/\Gamma t_\mathrm{e}\right]^2. \quad (6)$$

This form is only valid for $\tau > t_\mathrm{e}$. Note that a measurement made with a finite exposure time has an apparent contrast of $\beta' = \beta[\sinh(\Gamma t_\mathrm{e})/\Gamma t_\mathrm{e}]^2$ which is larger than would be measured for the same delay time with a negligibly short exposure time. Finally, note that in the limit of $\tau \to 0$ and $t_\mathrm{e} \to 0$ the contrast equals β, as it must.

Following along a similar line of reasoning, it is apparent that the variance of the intensity within a single exposure will also contain information about the intermediate scattering function. This is the basis of the technique known as speckle visibility spectroscopy (SVS) (Bandyopadhyay *et al.*, 2005). In particular, the normalized variance in the intensity, $V_2(t_\mathrm{e})$, as a function of the exposure time t_e is given by

$$V_2(t_\mathrm{e}) = \frac{\left\langle \bar{I}^2\right\rangle}{\langle I\rangle^2} - 1 = \frac{1}{\langle I\rangle^2}\frac{1}{t_\mathrm{e}^2}\left\langle \int_0^{t_\mathrm{e}}\int_0^{t_\mathrm{e}} I(t')I(t'')\,\mathrm{d}t'\,\mathrm{d}t''\right\rangle - 1. \quad (7)$$

Here, $\bar{I}$ refers to the intensity averaged over the exposure time. Equation (7) is equivalent to equation (4) for the limit of $\tau \to 0$. Note that V_2 is proportional to the square of the usual optics definition of visibility, which is why this is called visibility spectroscopy. Equation (7) can be simplified by writing it in terms of the intermediate scattering function,

$$V_2(t_e) = \frac{\beta}{t_e^2}\int_0^{t_e}\int_0^{t_e} f^2(t''-t')\,dt'\,dt''$$
$$= \frac{\beta}{t_e}\int_0^{t_e} 2(1-t/t_e)\,f^2(t)\,dt. \quad (8)$$

To obtain dynamics information about the sample one measures the variation of $V_2(t_e)$ as a function of t_e and then compares this with the predictions of (8) for a particular choice of $f(\tau)$. This suffers in comparison with XPCS where $f(\tau)$ is obtained directly, rather than only an integral over $f(\tau)$; however, it has the advantage of being able to resolve faster decay times as will be shown below. The replacement of $\langle I(t)I(t+\tau)\rangle$ by $1+f(\tau)$ in the formula for the speckle visibility assumes that the variance of the intensity is due entirely to speckle. In fact, photon statistics add an additional term to the variance as discussed by Dufresne *et al.* (1995). In the limit of weak scattering, which is typical for measurements with short exposure times, the contribution of photon statistics can be a significant modification. We avoid this complication by calculating the spatial correlation function of the intensity rather than the variance of the intensity itself. The spatial correlation function is given by

$$C(\Delta r) = \left\langle \bar{I}(r)\bar{I}(r+\Delta r)\right\rangle / \langle I\rangle^2. \quad (9)$$

In the limit that $\Delta r \rightarrow 0$ this correlation function approaches the normalized variance. As long as the exact condition of $\Delta r = 0$ is excluded, however, this correlation function does not include the photon statistics term. The way this is done practically is to resolve the intensity on the detector into individual photons and then measure the photon–photon spatial correlation function. Since this excludes the correlation of a photon with itself, the contribution from photon statistics is excluded. Consider the common case of the intermediate scattering function given by $f(\tau) = \exp(-\Gamma|\tau|)$. Putting this form into (8) yields

$$V_2(t_e) = \frac{\beta}{2\Gamma^2 t_e^2}\left[2\Gamma t_e - 1 + \exp(-2\Gamma t_e)\right]. \quad (10)$$

Note that, as with $f(0)$, $V_2(0) = \beta$, but unlike $f(\tau)$, which decays as an exponential for $\tau \rightarrow \infty$, the visibility decays, for long times, as $1/(\Gamma t_e)$.

3. Experiment

Dynamics measurements were made on suspensions of 72 nm-radius polystyrene latex spheres in glycerol. The latex suspension was originally obtained in water and then after addition of glycerol the water was evaporated in a rotary evaporator for a minimum of 8 h at 353 K to ensure removal of the water. Measurements were made on an 8% volume fraction suspension, where the corrections to simple Brownian motion due to volume fraction are minimal (Lurio *et al.*, 2000). The samples were sealed in 1 mm-outer-diameter borosilicate glass capillaries and epoxied onto a temperature-controlled sample holder. Sample temperatures were measured using a Pt resistance thermometer epoxied to the side of the glass capillaries close to the height at which the incident X-ray beam intercepted the sample.

Measurements were performed at the 8-ID-I experimental beamline at sector 8 of the APS (Sandy *et al.*, 1999). An APS undulator-A was set to select a first harmonic beam energy of 7.35 keV. Higher harmonics of the undulator were removed by reflection from a Si mirror 39.1 m upstream of the sample. The energy resolution was determined by reflection from a Ge double-bounce monochromator. The beam was unfocused in the horizontal direction and had a horizontal coherence length at the sample determined by the source size, σ_x, and source-to-sample distance, R, *via* $\xi_x = \lambda R/2\pi\sigma_x = 17$ µm (Sandy *et al.*, 1999). Here $\lambda = 0.166$ nm is the X-ray wavelength, $R = 68.2$ m and $\sigma_x = 110$ µm. The nominal horizontal source size is 287 µm but only part of the horizontal source is visible after reflection by the downstream mirror. The vertical coherence length at the sample is larger, 166 µm, owing to the smaller vertical source size of 11 µm. A defining slit, located 947 mm upstream of the sample, selected a horizontal beam size of 20 µm and a vertical beam size of 100 µm. Thus the beam, after passage through the defining slit, should be fully coherent in the vertical direction and partially coherent in the horizontal direction. A kinoform lens (Sandy *et al.*, 2007) with a focal length of 890 mm located 902 mm upstream of the sample focused the beam in the vertical direction. The diffraction-limited vertical spot size is a function of the vertical aperture at the sample and should be 1.5 µm FWHM, but was typically closer to 3 µm FWHM owing to imperfections in the optic. The purpose of focusing the vertical beam is to increase the speckle size of the scattering pattern. For a fixed total detector solid angle, the SNR depends linearly on the flux per speckle, and only as the square root of the number of speckles. Since a large speckle size distributes the same flux into fewer speckles, the SNR increases as the square root of the speckle size (Falus *et al.*, 2006).

The CCD camera was located a distance $R_d = 4.73$ m downstream from the sample. In the approximation that the beam is a monochromatic coherent plane wave with dimensions $W_{x,z}$ at the sample, and that the detector is in the far-field limit, the speckle size $\Delta_{x,z}$ at the camera is $\Delta_{x,z} = R_d\lambda/W_{x,z}$. Here, the x and z directions are normal to the beam. This relation yields 35 µm FWHM in the horizontal direction (approximately 1 pixel) and 235 µm FWHM in the vertical direction (approximately 8 pixels). A detailed treatment of speckle size based on Sandy *et al.* (1999) and Abernathy *et al.* (1998) yields results within 1% of these for the parameters used above.

For speckle visibility measurements the exposure time was varied using a resonant shutter manufactured by Electro-Optical Products Corporation. The resonant shutter consisted of an electrically driven mechanical resonator with shutter blades attached to each side of the resonating forks. Only one shutter blade was used to shutter the X-ray beam. The camera readout rate was phase-locked to the shutter. The exposure time of the camera could be varied by moving the beam vertically relative to the oscillating shutter blade position, thus

varying the fraction of the shutter period where the beam was occluded. The minimum exposure time was limited by the transit time of the shutter blade through the beam, which was of the order of 1 ms. XSVS measurements were made for exposure times of 2 ms, 5 ms and 10 ms. In order to minimize sample damage the capillary with the latex suspension was moved after approximately 10 s of exposure. Since this time is much longer than the relaxation time of the latex spheres (typically of the order of a few milliseconds), this occasional moving of the sample should have no significant effect on the measured sample dynamics.

4. Analysis of speckle pattern

The scattering from the latex suspension for an individual exposure was sufficiently weak that it could be resolved into individual photon droplets on the CCD camera. A single 2 ms exposure typically yielded around 50 scattered photons per frame. The center of mass for each photon charge droplet was obtained by analysis of the charge distribution on the camera, and each frame was converted into a list of photon positions. In the cases where photons overlapped, the positions were extracted using a non-linear least-squares fit to a sum of simulated charge droplets. Droplets consisting of more than three overlapping photons were thrown out as it was not possible to achieve sufficient noise suppression in these cases, and, in any case, such droplets constitute a negligibly small fraction of the droplets. The droplets were modeled by Gaussians. The amplitude and Gaussian widths of the simulated droplets in the horizontal and vertical directions were initialized at nominal average values and then allowed to vary to obtain the best fit to each droplet. A typical two-droplet charge pattern is shown in Fig. 1. Since measurements could involve of the order of 10^5 frames, the photon identification algorithm was computationally intensive and was performed using a 60 node parallel-processing cluster computer at Northern Illinois University. An image obtained by summing the droplets from 4096 separate frames is shown in Fig. 2.

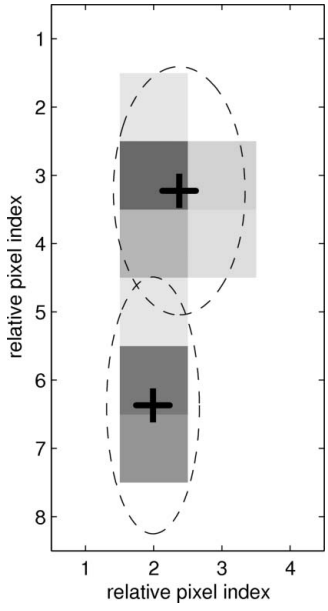

Figure 1
Typical fit to two photon charge droplets on the CCD camera. Ellipses show the outline of the 2σ charge boundary for Gaussian fits to the variance of the ADU signal in the x and y directions. Crosses show the centers of the droplets.

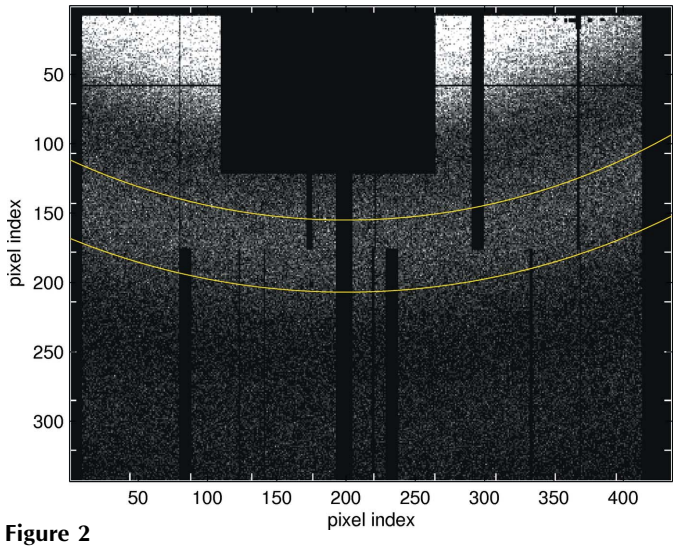

Figure 2
Sum of 4096 frames of data collected from the 72 nm latex colloid scattering. The region of data that was analyzed was between the two curves, $0.09\ \mathrm{nm}^{-1} < Q < 0.11\ \mathrm{nm}^{-1}$. This image shows the calculated photon positions, rather than raw pixel data. Defective regions in the CCD are masked out as shown. The large square mask at small Q (top center of the image) was used to exclude high-intensity regions from the analysis in order to avoid wasting computation cycles. The image shown used a 10 ms exposure time, and measured a sample at 293.9 K. The intensity near the center of the selected data region corresponds to approximately 8 photons pixel^{-1}.

The contrast of the scattering pattern was extracted through a spatial autocorrelation of the photon positions, averaged over all the measured frames. The spatial autocorrelation was calculated by counting the number of photons within a series of elliptical regions around each photon within a given frame. This correlation function was averaged over all photons in a frame and then over all frames. The spatial autocorrelation function was normalized to the cross spatial correlation between two frames separated by a long time delay. Specifically, for two frames A and B, the spatial cross correlation counted the number of photons in frame B within an ellipse of a given size around the position of a photon in frame A. When there is no speckle, the ratio of the same frame correlation function to the cross frame correlation function should be unity. When there is speckle, there will be a higher likelihood for photons within the same frame to be close together than photons in different frames. This method is equivalent to normalizing by setting $g_2(\tau) = 1$ for large τ, and thus does not allow for the possibility of static speckle. Ideally, it would be preferable to normalize the data to the azimuthal average of scattering within the same frame, since this would allow the measurement of static speckle. This method of normalization requires great care, however. The flat-field response of the camera must be carefully calibrated and the variation of the intensity over the width ΔQ of the azimuthal ring must be divided out. For the current measurement, where it was known

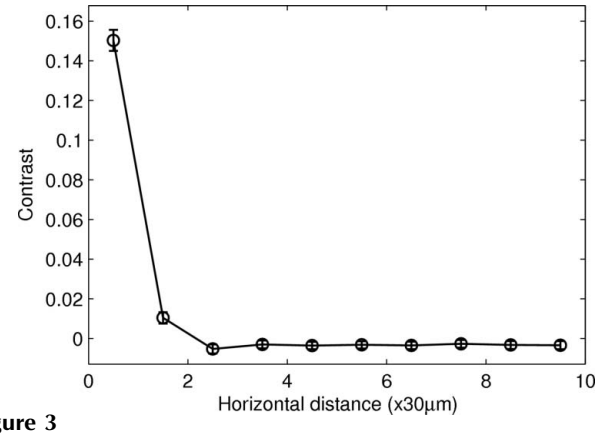

Figure 3
Photon spatial correlation function for 8% latex data, 2 ms exposure at 288 K. The correlations were made in elliptical regions with a vertical to horizontal ratio of 8:1. Data are averaged over 32000 frames.

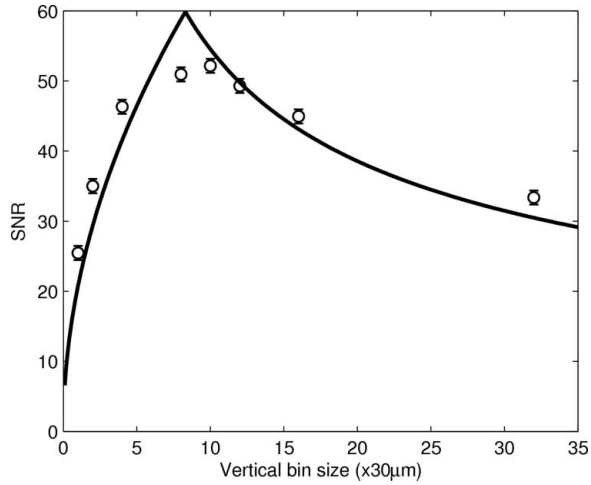

Figure 4
Signal-to-noise ratio as a function of vertical bin size. The SNR was calculated using scattering measured from 8% volume fraction latex colloids in glycerol at 258 K and using an exposure time of 10 ms. The line is the model described in the text.

that there was no static speckle, we did not attempt these detailed corrections.

A typical spatial correlation function is shown in Fig. 3. The photons were binned in elliptical regions, with the nth bin defined by $(n-1)^2 \leq (x/30\ \mu\text{m})^2 + (z/240\ \mu\text{m})^2 \leq n^2$. Except for the first two bins, the ratio of the self to cross correlation is close to unity. The first bin shows an excess of contrast of 14% indicating the presence of speckle. The uncertainty in the correlation function, indicated by the error bars in the figure, was calculated from the square root of the number of photons in each bin. While we did not perform a detailed analysis of the effect of the focusing optic on the coherence, we can estimate the expected contrast under the *ad hoc* assumption that the fraction of vertical coherence at the defining slit upstream of the kinoform lens is preserved in the focus of the lens. Under this assumption the vertical beam size is scaled down from 100 μm at the defining slit to 3 μm at the focus and the coherence length is similarly scaled down to ξ_z = 5 μm. Using the relations for the contrast given by Sandy *et al.* (1999), the estimated contrast would be 41% rather than the measured 14%. We attribute the difference to imperfections in the focusing optic. Note, however, that even with only 34% of the expected contrast and a kinoform efficiency of ∼50% the expected SNR is still approximately ten times better than what would be achieved without vertical focusing.

The SNR can be measured from the ratio of the contrast to the uncertainty in the magnitude of the central point in the spatial correlation function. This ratio will depend on the size of the binning regions used to calculate the spatial correlation function. If the bins are too large the contrast will decrease, while if the bins are too small the error bar will increase. The SNR should be maximized when the binning size matches the speckle size in the horizontal and vertical directions. Optimization of the horizontal bin size yielded an optimum value of approximately 1 pixel (30 μm). For vertical binning, the SNR was optimized for a bin size of approximately 8 pixels as indicated in Fig. 4. If b_0 is the optimal bin size, we expect the SNR to vary approximately as $(b/b_0)^{1/2}$ for $b < v_0$ and as $(b_0/b)^{1/2}$ for $b > b_0$. This model is plotted as the line in Fig. 4. It yields a reasonable description of the SNR dependence on b. A more accurate model would require an integral over the speckle shape on the detector. The optimal horizontal bin size was comparable with the expected value. The optimal vertical bin size is approximately two times smaller than expected for a 1.5 μm vertical focus, indicating that the kinoform focus was approximately two times larger than the diffraction limit of the optic.

In order to measure dynamics at delay times longer than 10 ms, cross-correlation functions were calculated as a function of frame offset. This method is essentially identical to traditional XPCS but is more amenable to dealing with the scattering stored as a list of photon positions rather than as intensity values binned into pixels. An alternative would be to place the photons into the nearest pixel and proceed with a standard XPCS analysis. This would, however, have had two disadvantages: first, the photons positions determined from the center of mass of the charge droplets can be located to better resolution than the size of a pixel, thus re-placing the photons into pixels would throw away this information; second, binning the data into histograms allows for optimizing the speckle size as an ellipse, while binning pixels together forces the speckles to be approximated by rectangular regions.

5. Dynamics measurements

XSVS measurements as well as XPCS measurements were made on an 8% volume fraction suspension of 72 nm-radius latex nanoparticles as a function of temperature. Dilute suspensions of spherical particles should execute Brownian diffusion with an intermediate scattering function given by $f(Q, \tau) = \exp(-\Gamma|\tau|)$. Here the relaxation time is given by $\Gamma = DQ^2$. The diffusion constant for a spherical particle of radius r in a suspension of viscosity η is given by the Stokes–Einstein relationship,

$$D = k_B T/6\pi\eta r. \quad (11)$$

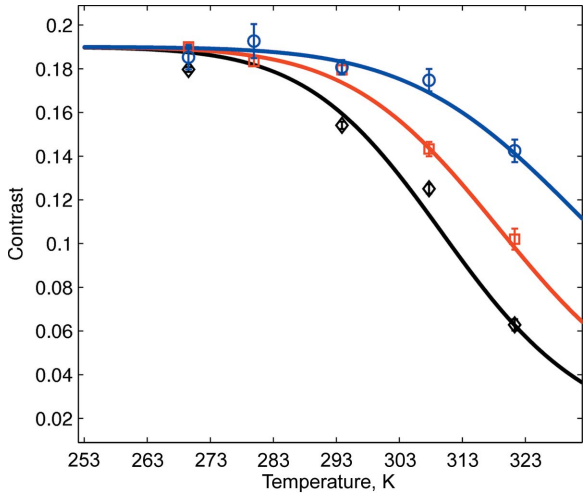

Figure 5
Speckle visibility contrast as a function of temperature for 72 nm-radius latex in glycerol; the data shown were collected at a wavevector transfer of $Q = 0.1 \pm 0.01$ nm^{-1}. Blue circles: 2 ms exposure; red squares: 5 ms exposure; black diamonds: 10 ms exposure. The 2 ms data are multiplied by a factor of 1.039 to account for the reduced contrast resulting from the shutter transit time. Solid lines are theoretical predictions based on Brownian motion.

The viscosity of glycerol has a strong temperature dependence and varies by over a factor of a thousand over the range of temperatures measured. Thus, by varying the temperature of the glycerol, the relaxation time of the latex suspension could be varied over a wide range.

Speckle visibility *versus* temperature is shown in Fig. 5. Data are shown at an average $Q = 0.10 \pm 0.01$ nm^{-1} for three different exposure times, 2 ms, 5 ms and 10 ms, over a range of temperature from 269.55 K to 321.3 K. The visibility for the 5 ms and 10 ms exposures are unmodified from the values obtained from the spatial correlation functions as described above. The visibility of the 2 ms data was multiplied by a correction factor of 1.039. The cause of this contrast correction was that the transit time of the shutter through the beam is of the order of 1 ms, which is a significant fraction of the 2 ms exposure time. During the time when the shutter edge cuts the beam, the beam height on the kinoform lens is reduced, leading to a larger focal point size and consequently smaller speckles. The transit time of the shutter was sufficiently small that this effect did not significantly effect the 5 ms or 10 ms data. The theoretical curves shown in Fig. 5 were calculated using equations (10) and (11). Two adjustable parameters were used to fit the 14 data points, one for the limiting contrast of the 5 ms and 10 ms exposures, and the second for the limiting contrast of the 2 ms exposures. Thus the good agreement between the data and the model indicate that the visibility is a useful measure of the relaxation time.

One can also compare the dynamics as measured using speckle visibility with the dynamics measured using XPCS through frame cross correlation. Figs. 6(*a*) and 6(*b*) show speckle visibility contrast for 2 ms, 5 ms and 10 ms exposures. Also shown are the XPCS data obtained from cross correlation of the 10 ms exposures. The theoretical curves are from equation (10) for the visibility data and equation (6) for the cross-correlation data. The 2 ms exposures were multiplied by the same correcting factor used for the fits in Fig. 5. Data are shown at two temperatures, 293.9 K, where there is still significant contrast left for XPCS, and 307.7 K, where the XPCS visibility is almost gone. With no adjustable parameters the XPCS and SVS data give good agreement with theory using the same relaxation time.

6. Discussion

Speckle visibility spectroscopy is an alternative method to X-ray photon correlation spectroscopy that can be used to obtain information about the intermediate scattering function $f(Q, \tau)$. When $f(Q, \tau)$ is represented by an exponential decay, the speckle visibility has a straightforward analytic form that fits well to experimental data for the Brownian diffusion of colloidal particles. A number of other analytic forms are given by Bandyopadhyay *et al.* (2005). Speckle visibility obviously has limitations when the form of $f(Q, \tau)$ is not known, since all that is measured in that case is an integral over the intermediate scattering function. However, it has the significant advantage that the contrast falls off significantly slower with time than in the case of photon correlation spectroscopy.

Considering the graphs in Fig. 6, if the 1/*e* point of the XPCS and SVS curves are compared, the SVS method can access four times faster dynamics with equal exposure times. The key point is that by using a resonant shutter to further reduce the exposure time we have been able to probe dynamics a factor of 20 faster than could be done using frame-to-frame correlations, while still maintaining the advantage of multi-speckle measurements using a CCD camera. For the current measurement the shutter transit time of 1 ms limited the

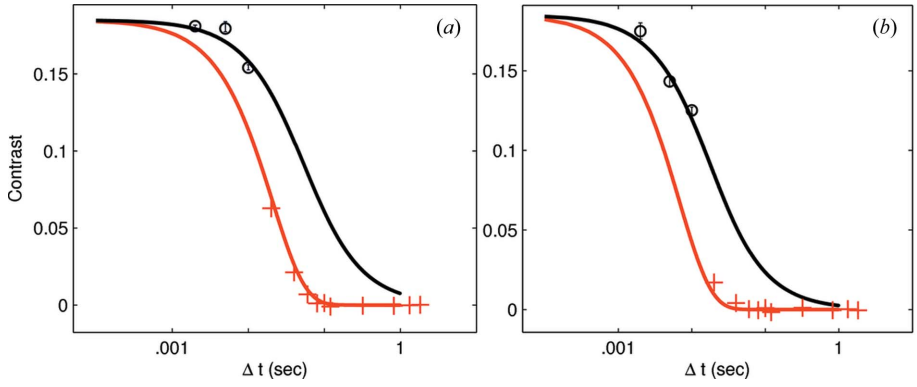

Figure 6
Combined speckle visibility contrast and XPCS contrast at (*a*) 293.9 K and (*b*) 307.7 K for 72 nm latex; data shown were collected at a wavevector transfer of $Q = 0.1 \pm 0.01$ nm^{-1}. The data are shown as V_2 and as $g_2 - 1$ for the XPCS data. The SVS points at 2 ms, 5 ms and 10 ms are shown as circles. The XPCS data were obtained from the cross correlation of the 10 ms data and are shown as crosses. The solid lines are the fits as described in the text.

minimum exposure time. This limitation can be overcome by relocating the position of the shutter in the beamline and a factor of ten increase in shutter speed should be obtainable, allowing access to submillisecond dynamics. The visibility method also has advantages with regards to sample damage, as it would be possible in principle to move the sample between every exposure. This would limit the exposure time for a single spot on a sample to milliseconds. Finally, we point out that the technique discussed here works with extremely low count rates. For the 2 ms exposures, the average flux was 2×10^{-4} photons pixel^{-1} exposure^{-1} or 1×10^{-3} photons speckle^{-1} exposure^{-1}. This is significantly less than the sometimes stated rule of thumb that PCS requires one photon per speckle per correlation time. The ability to measure at low flux is due to averaging over a large number of independent measurements, typically of the order of 10^8 speckles. Thus, even with the current intensity levels of undulator sources, XSVS can make submillisecond measurements possible with large high-resolution detectors and sufficient patience.

We would like to acknowledge the assistance of Raymond Ziegler for help at sector 8-ID-I of the Advanced Photon Source. This work was supported by DOE grant DE-SC0005135. Use of the Advanced Photon Source at Argonne National Laboratory was supported by the US Department of Energy, Office of Science, Office of Basic Energy Sciences, under DOE Contract No. DE-AC02-06CH11357.

References

Abernathy, D. L., Grübel, G., Brauer, S., McNulty, I., Stephenson, G. B., Mochrie, S. G. J., Sandy, A. R., Mulders, N. & Sutton, M. (1998). *J. Synchrotron Rad.* **5**, 37–47.

Bandyopadhyay, R., Gittings, A. S., Suh, S. S., Dixon, P. K. & Durian, D. J. (2005). *Rev. Sci. Instrum.* **76**, 093110.

Chushkin, Y., Caronna, C. & Madsen, A. (2012). *J. Appl. Cryst.* **45**, 807–813.

Denes, P., Doering, D., Padmore, H. A., Walder, J. P. & Weizeorick, J. (2009). *Rev. Sci. Instrum.* **80**, 083302.

Dufresne, E., Bruning, R., Sutton, M., Rodricks, B. & Stephenson, G. B. (1995). *Nucl. Instrum. Methods Phys. Res. A*, **364**, 380–393.

Falus, P., Borthwick, M. A. & Mochrie, S. G. J. (2004). *Rev. Sci. Instrum.* **75**, 4383.

Falus, P., Lurio, L. B. & Mochrie, S. G. J. (2006). *J. Synchrotron Rad.* **13**, 253–259.

Grubel, G., Madsen, A. & Robert, A. (2008). In *Soft-Matter Characterization*, edited by R. Borsali and R. Pecora. Heidelberg: Springer.

Hruszkewycz, S. O., Sutton, M., Fuoss, P. H., Adams, B., Rosenkranz, S., Ludwig, K. F., Roseker, W., Fritz, D., Cammarata, M., Zhu, D., Lee, S., Lemke, H., Gutt, C., Robert, A., Grübel, G. & Stephenson, G. B. (2012). *Phys. Rev. Lett.* **109**, 185502.

Livet, F., Bley, F., Mainville, J., Caudron, R., Mochrie, S., Geissler, E., Dolino, G., Abernathy, D., Bel, G. G. & Sutton, M. (2000). *Nucl. Instrum. Methods Phys. Res. A*, **451**, 596–601.

Lurio, L. B., Lumma, D., Sandy, A. R., Borthwick, M. A., Falus, P., Mochrie, S. G., Pelletier, J. F., Sutton, M., Regan, L., Malik, A. & Stephenson, G. B. (2000). *Phys. Rev. Lett.* **84**, 785–788.

Pecora, R. (1985). *Dynamic Light Scattering: Applications of Photon Correlation Spectroscopy*. New York: Plenum Press.

Pusey, P. N. (1991). In *Liquids Freezing and the Glass Transition*, edited by J. P. Hansen, D. Levesque and J. Zinn, ch. 10. Amsterdam: Elsevier.

Sandy, A. R., Evans-Lutterodt, K., Fezzaa, K., Kim, S., Narayanan, S., Sprung, M. & Stein, A. (2007). *Proc. SPIE*, **6705**, N7050.

Sandy, A. R., Lurio, L. B., Mochrie, S. G. J., Malik, A., Stephenson, G. B., Pelletier, J. F. & Sutton, M. (1999). *J. Synchrotron Rad.* **6**, 1174–1184.

Westermeier, F., Autenrieth, T., Gutt, C., Leupold, O., Duri, A., Menzel, A., Johnson, I., Broennimann, C. & Grübel, G. (2009). *J. Synchrotron Rad.* **16**, 687–689.